Vortex-solid melting and depinning in superconducting Y-Ba-Cu-O single crystals irradiated by 3-MeV protons

W. Jiang, N.-C. Yeh, D. S. Reed, U. Kriplani, T. A. Tombrello, and A. P. Rice
Department of Physics, California Institute of Technology, Pasadena, California 91125

F. Holtzberg
IBM Research Division, Thomas J. Watson Research Center, Yorktown Heights, New York 10598

(Received 14 December 1992)

The effects of controlled point defects on the vortex-solid melting and depinning of high-temperature superconductors are investigated by applying the critical scaling analysis to the vortex transport properties of 3-MeV-proton-irradiated Y-Ba-Cu-O single crystals. For magnetic fields ranging from 1 kOe to 90 kOe, the critical exponents of the melting transition are found to be *universal*, independent of the density of point defects. In contrast, material parameters associated with the vortex depinning are modified by the proton irradiations.

Among various theories of the vortex transport in high-temperature superconductors (HTS),[1,2] a second-order vortex-solid melting transition has been proposed as the mechanism for the onset of vortex dissipation in the weak pinning limit.[1] The experimental evidence for such a phase transition has been manifested by the universal critical scaling behavior of the vortex transport properties obtained from both dc and ac transport measurements.[3–6] Since a dislocation-mediated melting transition is insensitive to the density of randomly distributed weak-pinning point defects, the vortex dissipation near the melting transition should be governed by the same critical phenomena, independent of moderate variations in the density of point defects. In this paper we report studies of the vortex critical fluctuations on 3-MeV-proton-irradiated superconducting Y-Ba-Cu-O single crystals. In contrast to previous magnetization studies on similarly prepared samples,[7] this work focuses on the vortex transport properties in the *critical regime* of the vortex-solid melting transition. For magnetic fields ranging from 1 to 90 kOe, we find that a well-defined second-order melting transition remains despite the significant increase of point defects after proton irradiations; the vortex transport properties near the melting transition of all samples are governed by the *same* critical exponents ($\nu \approx 2/3$ and $z \approx 3$). Since a given class of second-order phase transitions should be characterized by certain *universal* critical exponents, our finding of consistent critical exponents for samples with different densities of point defects provides strong support for the accuracy of these exponents. In addition, we find that the pinning-related material parameters are modified upon irradiation; the zero-field superconducting transition temperature and the vortex correlation length *decrease* with the increasing disorder; the high-field melting transition temperature and the flux-flow crossover current density *increase* with the increasing point defects.

The parent sample used for proton irradiations is a well-characterized twinned Y-Ba-Cu-O single crystal with a zero-field transition temperature $T_{c0}=92.95\pm0.05$ K, 100% superconducting volume, normal-state resistivity at T_{c0} of 55 $\mu\Omega$ cm, and sample dimensions $0.90\times0.65\times0.021$ mm^3, as described in Ref. 8. The irradiations with 3-MeV protons are performed at room temperature using a tandem Van de Graaff accelerator, with the beam orientation parallel to the c axis of the sample. The sample is irradiated twice, with a fluence of 5×10^{15} protons/cm^2 each time. Since the range of 3-MeV protons in Y-Ba-Cu-O is about 45 μm, greater than the crystal thickness (21 μm), all incident protons can pass completely through the sample. The defects created by 3-MeV protons are randomly distributed point defects with volume density $\sim1.1\times10^{19}$ cm^{-3} for the fluence of 5×10^{15} protons/cm^2 (Ref. 9). This estimate is in good agreement with that obtained by Monte Carlo simulations.[7] Following each proton irradiation, dc transport measurements are carried out using the standard four-probe method in magnetic fields H ranging from 1 to 90 kOe, with H perpendicular to the applied current density **J**, and for H both parallel and perpendicular to the c axis of the sample. Details of the sample characterizations and experimental techniques are given in Ref. 8. In the following we concentrate on the data analysis to compare the vortex transport properties for samples with and without proton irradiation. For convenience, we denote the samples before the irradiation, after the first irradiation, and after the second irradiation as samples A, B, and C, respectively. The T_{c0} values for samples A, B, C are shown in Table I.

Near a second-order vortex-solid melting transition temperature $T_M(H)$ and in the low current density limit, we may define a vortex correlation length ξ which follows the temperature dependence[1,3]

$$\xi=\xi_0(H)|1-T/T_M(H)|^{-\nu}\ , \tag{1}$$

where ν is the static exponent, and ξ_0 is a temperature-independent constant. In a constant H, the electric field E due to the vortex dissipation near T_M yields the critical scaling relation[1,3]

$$E=J\xi^{(z-1)}\tilde{E}_\pm(x),\quad x\equiv J\xi^2\Phi_0/(k_BT)\ , \tag{2}$$

where z is the dynamical critical exponent, and $\tilde{E}_\pm(x)$ are

TABLE I. The proton fluence f dependence of the zero-field transition temperature T_{c0}, the zero-field critical exponents $\nu_{0\parallel}$ ($\mathbf{H}\parallel c$) and $\nu_{0\perp}$ ($\mathbf{H}\perp c$), and the power a for the flux-flow crossover current density $J_x(T)$ (see text).

Sample	f (protons /cm^2)	T_{c0} (K)	ν_0 $\nu_{0\parallel}$	$\nu_{0\perp}$	a
A	0	92.95±0.05	0.65	0.65	0.62
B	$\sim 5\times10^{15}$	92.25±0.05	0.63	0.64	0.58
C	$\sim 1\times10^{16}$	91.62±0.05	0.62	0.63	0.67

the universal functions for $T>T_M(\tilde{E}_+)$ and $T<T_M(\tilde{E}_-)$, respectively. Defining $\tilde{E}=(E/J)|1-(T/T_M)|^{\nu(1-z)}$ and $\tilde{J}\equiv(J/T)|1-(T/T_M)|^{-2\nu}$, we can "collapse" *all* E vs J isotherms within the critical regime[3] into two universal curves $\tilde{E}_\pm$ with proper values of T_M,ν and z. Figure 1 shows two sets of representative E vs J isotherms and the corresponding universal functions for samples B and C. We find that for both samples in two magnetic-field orientations ($\mathbf{H}\parallel c$ and $\mathbf{H}\perp c$), and for H ranging from 1 to 90 kOe, the critical scaling analysis in Eq. (2) gives *universal* critical exponents $\nu=0.65\pm0.05$ and $z=3.0\pm0.3$, which are consistent with the results for sample A obtained from both dc and ac transport measurements.[3,4] Furthermore, the universal functions $\tilde{E}_\pm(x)$ for all three samples in all fields are also identical, except for a nonuniversal constant that provides information about the vortex correlation length $\xi_0(H)$ (Ref. 3). Consequently, the universal scaling behavior of vortex transport properties in HTS samples with different densities of weak pinning defects is for the first time unambiguously demonstrated, lending further strong support for a dislocation-mediated second-order phase transition.

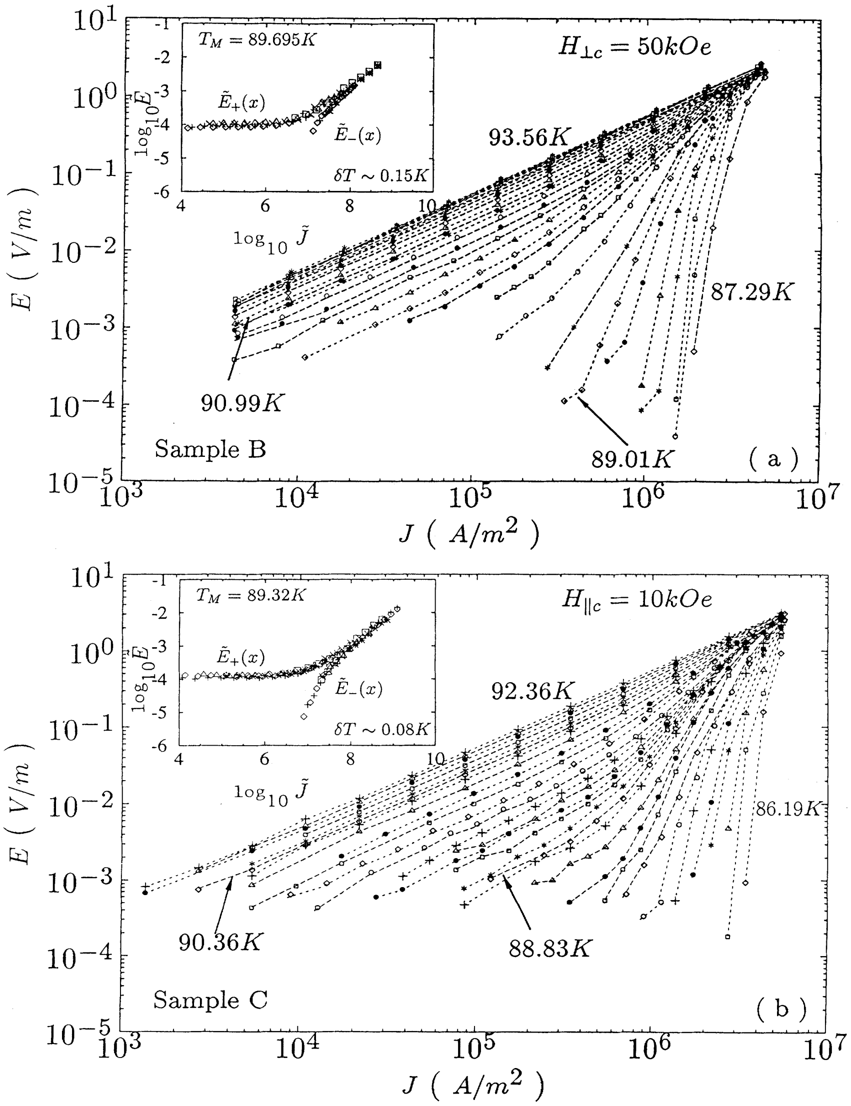

FIG. 1. Representative electric field E vs current density J isotherms. (a) Sample B with $\mathbf{H}\perp$ c axis and $H=50$ kOe. (b) Sample C with $\mathbf{H}\parallel$ c axis and $H=10$ kOe. The insets are the universal functions $\tilde{E}_\pm(x)$ obtained from collapsing the isotherms with $J_l(T,H)<J<J_c(T,H)$ and T within the critical regime indicated by the arrows. The parameters used for the collapsing are $\nu=0.67$, $z=3.0$ and the $T_M(H)$ values indicated in the insets. δT is the averaged temperature increment of the isotherms in the critical regime.

The melting transition temperatures $T_M(H)$ obtained by using Eq. (2) are plotted in Fig. 2 for all three samples. We note that all melting lines follow the same relation $H_M(T)=H_M(0)|1-(T/T_{c0})|^{2\nu_0}$, with $\nu_0=0.63\pm0.02$ (see Table I), consistent with a 3D *XY* model which asserts $\nu_0=(2/3)$ (Ref. 1). Interestingly, however, the high-field melting temperatures for both $H\|c$ and $H\perp c$ increase with the increasing disorder (see Fig. 2) despite the decrease in T_{c0}. The vortex correlation length $\xi_0(H)$ in a given magnetic field decreases with the increasing density of point defects, as shown in Fig. 3(a) for both $H\|c$ and $H\perp c$. The decrease of ξ_0 may be attributed to the smaller vortex loops in the presence of larger densities of point defects after proton irradiations. The inset of Fig. 3(a) shows that $\xi_0(H\|c)\approx\xi_0(H\perp c)$ is within the experimental error, consistent with our definition of the vortex correlation length as the mean value of those along the *c* axis and the *ab* plane.[3]

We note that the above critical scaling analysis is valid only if the applied current density J is smaller than the critical current density and if the sample size is infinite.[3] In the presence of finite-size effects, the current range for observing the critical scaling behavior is further limited by a lower bound (Ref. 3). That is, the critical scaling behavior of the vortex dissipation breaks down when $J<J_l$, where l is the "vortex mean free path".[3] In a twinned single crystal, $l(H)=L_t-r_p(H)$, where L_t is the average twin boundary separation and $r_p(H)$ is the twin boundary pinning range. When $\xi\rightarrow l$ as $T\rightarrow T_M$, the twin-boundary pinning limits the long-range vortex correlation, so that pinning becomes dominant, and the critical scaling relation breaks down.

Experimentally, for a constant H, J_l can be obtained by identifying the current density below which the E vs J isotherm deviates from the critical scaling expression in Eq. (2). The physical meaning of J_l is associated with the work ($J_l l^2\Phi_0$) done on the vortex dislocation loop by the Lorentz force. In the steady state, the total thermal energy k_BT of each dislocation loop is equal to the sum of the work done by the Lorentz force and by the pinning force on the dislocation loop, i.e.,

$$J_l l^2\Phi_0-W_p=k_BT \ . \tag{3}$$

Given a volume density n_p of randomly distributed point defects, it is known that the pinning energy W_p satisfies $W_p\propto n_p$ if the single-particle pinning dominates.[10] In the $n_p\rightarrow 0$ limit, we recover the result in Ref. 3 which yields

$$J_l(T_M,H)=k_BT_M(H)/(l^2\Phi_0) \ .$$

Our results [the inset of Fig. 3(b)] show that the vortex mean free path $l(H)$ decreases with the increasing magnetic field, consistent with the fact that L_t is constant and the twin-boundary pinning range $r_p(H)$ increases with the increasing density of vortices. Furthermore, since $l(H)$ is independent of n_p, and experimentally J_l increases with the increasing n_p, it follows from Eq. (3) that the pinning energy W_p increases with the increasing n_p. Inserting the values of $l(H)$, $T_M(H)$, and $J_l(T_M,H)$ into Eq. (3), we obtain the $W_p(T_M,H)$ vs H data for samples B and C, as shown in Fig. 3(b). Note that $(W_p)_C\approx 2(W_p)_B$, consistent with $W_p\propto n_p$.

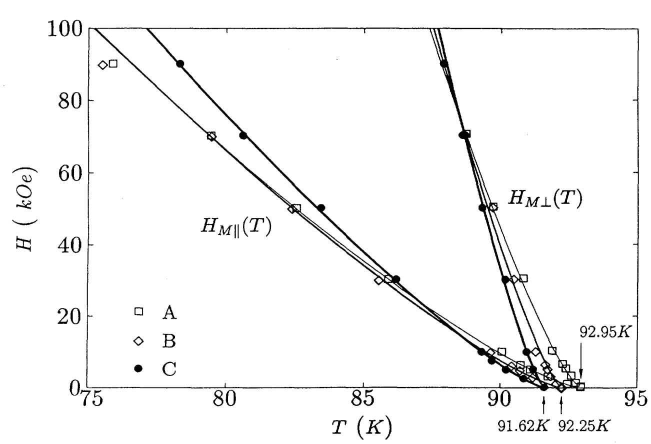

FIG. 2. The anisotropic vortex-solid melting transition lines for H$\|$ *c* axis [$H_{M\|}(T)$] and H$\perp$ *c* axis [$H_{M\perp}(T)$], and for samples A, B, C. All solid lines satisfy the relation $H_M(T)=H_M(0)|1-T/T_{c0}|^{2\nu_0}$ with ν_0 values given in Table I.

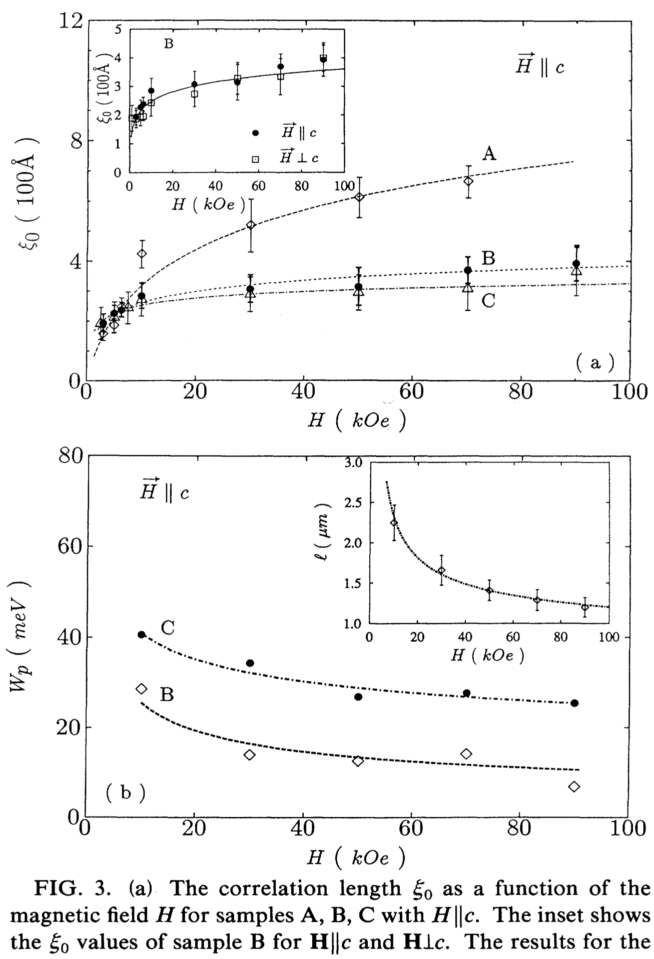

FIG. 3. (a) The correlation length ξ_0 as a function of the magnetic field H for samples A, B, C with $H\|c$. The inset shows the ξ_0 values of sample B for H$\|c$ and H$\perp c$. The results for the other two samples are similar in that $\xi_0(H)$ values are the same for the two H orientations within experimental errors. (b) The pinning energy W_p as a function of the magnetic field H for samples B and C. Note that $(W_p)_C\approx 2(W_p)_B$. The inset shows the vortex mean free path $l(H)$ obtained from sample A and for H$\|c$.

The flux-flow crossover current density $J_x(T)$ places an upper current limit for the validity of Eq. (2), so that for $J>J_x(T)$, the superconducting system is in the flux-flow regime[2] with ohmic vortex dissipation. Experimentally J_x at a constant temperature can be obtained by identifying the current density of an E vs J isotherm above which the isotherm becomes ohmic. The J_x vs the reduced temperature (T/T_{c0}) curves for all three samples are shown in Fig. 4. There are two important features associated with the flux-flow critical current densities. First, the fitting curves (the dashed lines) in Fig. 4 all follow the relation $J_x(T)=J_x(0)|1-(T/T_{c0})|^a$, where a is very close to ν_0, as shown in Table I. Second, the magnitude of $J_x(0)$ is independent of H and is significantly enhanced for the irradiated samples. One possible explanation for the magnitude and the temperature dependence of $J_x(T)$ is as follows. The flux-flow crossover current density can be related to the single vortex pinning energy (U_p) by the relation $U_p=(J_x\Phi_0 rL)$, where Φ_0 is the flux quantum, L is the length of a flux line, and r is the pinning range. Furthermore, U_p is approximately equal to the condensation energy $[B_c^2 V_c/(2\mu_0)]$, where B_c is the thermodynamic critical field (measured in tesla), μ_0 is the vacuum permeability, $V_c \sim \xi_s^3$ is the correlation volume per vortex in the flux-flow limit, and $\xi_s(T)=\xi_s(0)|1-(T/T_{c0})|^{-\nu_0}$ is the superconducting coherence length. (We have neglected the anisotropy for simplicity.) Since $B_c^2 \approx \Phi_0^2/(8\pi^2\kappa^2\xi_s^4)$, where κ is the Ginzburg-Landau parameter, we find that

$$J_x(T)=\frac{\Phi_0}{16\mu_0\pi^2 rL\kappa^2\xi_s(0)}\left[1-\frac{T}{T_{c0}}\right]^{\nu_0}. \tag{4}$$

Consequently, we have $a=\nu_0\approx 2/3$, consistent with the experimental observation, provided that r and L are only weakly dependent on the temperature and the magnetic field. (For instance, r could be the average size of a point defect and L could be the thickness of the sample). In addition, since $J_x(0)\propto 1/\kappa^2$ from Eq. (4), and since $\kappa=(\lambda_{\text{eff}}/\xi_s)$, where λ_{eff} is the effective penetration depth, we find that for $\lambda_{\text{eff}}=\lambda_C=\sqrt{c_{44}/k_p}$, with λ_C being the Campbell penetration depth (Ref. 11), c_{44} the tilt modulus, and k_p the Labusch pinning force constant,[12] κ decreases with the increasing pinning force constant k_p. Therefore $J_x(0)\propto k_p$, consistent with the observation of increasing J_x with the increasing strength and density of pinning. It is worth noting that the flux-flow crossover current density J_x defined in this work is different from the "magnetic" critical current densities J_c of similarly prepared samples.[7] The J_c values in Ref. 7 were obtained by using Bean's critical-state model[13] and the relation $\mathbf{J}_c=(\nabla\times\mathbf{h})$, where $\mathbf{h}$ is the local magnetic field inside the sample. Consequently the J_c values are related to the magnetic irreversibility of vortices in the flux-creep limit,[2] and are dependent on the applied field H and the effective penetration depth.

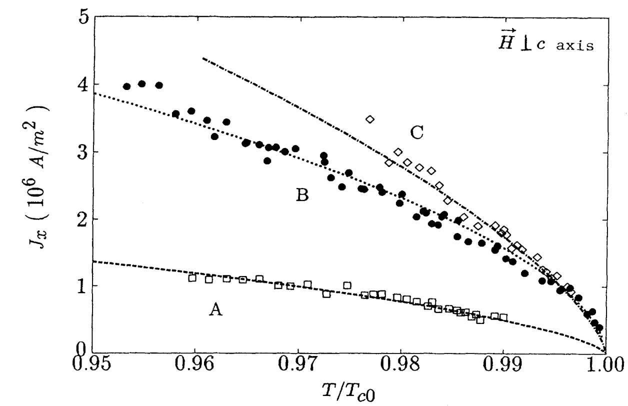

FIG. 4. The flux-flow crossover current density (J_x) vs the reduced temperature (T/T_{c0}) for samples A, B, C and $\mathbf{H}\perp c$ axis. Note that J_x is independent of the magnetic field.

In summary, we have investigated the critical phenomena of the vortex transport properties in 3-MeV-proton-irradiated Y-Ba-Cu-O single crystals. We find that the onset of vortex dissipation is consistent with a second-order vortex-solid melting transition, with *universal* critical exponents $\nu\approx 2/3$ and $z\approx 3$, independent of the density of point defects. On the other hand, the increase of point defects modifies the pinning-related material parameters; the zero-field transition temperature T_{c0} and the vortex correlation length ξ_0 decrease with the increasing defect density, while the flux-flow crossover current density J_x and the high-field melting transition temperature (T_M) increase with the increasing defects.

We thank Nils Asplund for his technical assistance. This work is jointly supported by ONR Grant No. N00014-91-1556, NASA/OAET, IBM-Caltech Cooperative Research Fund, and NSF Grant No. DMR90-11230.

[1] D. S. Fisher, M. P. A. Fisher, and D. Huse, Phys. Rev. B **43**, 130 (1991).
[2] E. H. Brandt, Int. J. Mod. Phys. B **5**, 751 (1992).
[3] N.-C. Yeh, W. Jiang, D. S. Reed, U. Kriplani, and F. Holtzberg, Phys. Rev. B **47**, 6146 (1993); Mat. Res. Soc. Symp. Proc. **275**, 169 (1992).
[4] D. S. Reed, N.-C. Yeh, W. Jiang, U. Kriplani, and F. Holtzberg, Phys. Rev. B **47**, 6150 (1993); Mat. Res. Soc. Symp. Proc. **275**, 413 (1992).
[5] R. H. Koch *et al.*, Phys. Rev. Lett. **63**, 1511 (1989); H. K. Olsson *et al.*, *ibid.* **66**, 2661 (1991).
[6] P. L. Gammel *et al.*, Phys. Rev. Lett. **66**, 953 (1991).
[7] L. Civale, A. D. Marwick, M. W. McElfresh, A. P. Malozemoff, and F. Holtzberg, Phys. Rev. Lett. **65**, 1164 (1990).
[8] N.-C. Yeh, D. S. Reed, W. Jiang, U. Kriplani, F. Holtzberg, A. Gupta, B. D. Hunt, R. P. Vasquez, M. C. Foote, and L. Bajuk, Phys. Rev. B **45**, 5654 (1992).
[9] M. W. Thompson, *Defects and Radiation Damage in Metals* (Cambridge University, Cambridge, England, 1969), p. 113.
[10] A. I. Larkin and Yu. N. Ovchinnikov, J. Low Temp. Phys. **34**, 409 (1978).
[11] A. M. Campbell, J. Phys. C **2**, 1492 (1969); **4**, 3186 (1971).
[12] A. M. Campbell and J. E. Evetts, Adv. Phys. **21**, 199 (1972).
[13] C. P. Bean, Phys. Rev. Lett. **8**, 250 (1962).